Results in Optics 10 (2023) 100365

Contents lists available at ScienceDirect

Results in Optics

journal homepage: www.sciencedirect.com/journal/results-in-optics

Luminescence of AlN:Mn^{2+} materials: Properties and mechanisms

R. Ruska [a], B. Berzina [a,*], J. Cipa [a], L. Trinkler [a], A. Sarakovskis [a], J. Grabis [b], I. Steins [b]

[a] Institute of Solid State Physics, University of Latvia, 8 Kengaraga Str., Riga LV-1063, Latvia
[b] Institute of Inorganic Chemistry, Riga Technical University, 3 P. Valdena Str., Riga LV-1048, Latvia

ARTICLE INFO

Keywords:
Manganese doped aluminum nitride
Ceramics
Nanopowder
Photoluminescence and excitation spectra
Luminescence kinetics
Luminescence mechanisms
Persistent luminescence

ABSTRACT

Luminescence processes resulting in 600 nm emission of Mn^{2+} ions in AlN:Mn ceramics were studied based on investigations of photoluminescence and its excitation spectra, luminescence kinetics and long-lasting luminescence (PersL) properties. For AlN:Mn^{2+} nanopowders, the photoluminescence spectra and PersL were studied. Luminescence properties were examined and compared after the samples were irradiated with 520 nm light, resulting in direct excitation of Mn^{2+} ions, thus causing the intra-center luminescence, or with 263 nm light. As known, in the last case, the oxygen-related defects are primarily excited with the following energy transfer to Mn^{2+} ions and 600 nm emission, thus forming the recombination luminescence (RecL). Two types of excitations of the 600 nm RecL were used. In the first case, the luminescence response was detected during the sample irradiation with 263 nm light. It was found that at RT, the decay of the RecL is fast and its decay constant $\tau = 1.2$ ms coincides with the value obtained for the intra-center luminescence. A time-dependent rise of the 600 nm luminescence intensity under 263 nm excitation was observed. In the other case, the 600 nm RecL was detected when irradiation of the sample with 263 nm light was ceased, and spectra and decay of PersL were studied. It was found that the decay of 600 nm PersL spectra could be described using three exponential functions, thus manifesting a variety of luminescence processes. The results allow tracing of the luminescence processes and proposal of the mechanisms resulting in the 600 nm light emission of Mn^{2+} ions. An energy level scheme of AlN:Mn^{2+} was constructed to elucidate of the luminescence processes and mechanisms.

1. Introduction

Today, solid-state luminescent materials are widely used and the need for unique products with distinct characteristics is growing. Their use ranges from lighting to optical sensors and innovative light emitters with a focus on the far-ultraviolet (F-UV) and red-infrared (R-IR) spectral regions. The R-IR emitters are prospective for biomedical applications (Wu et al., 2020; Zhuang et al., 2014). Single or compound metal oxides, nitrides, and related materials doped with rare-earth or transition metal ions are common types of solid-state UV–visible-IR light emitters. Among various dopants, manganese (Mn) ions are known as red light emitters, when incorporated in different types of host materials for which a high electrical field in the crystalline lattice is characteristic (Ni et al., 2018; Tanaka et al., 2000; Lei et al., 2004; Hou et al., 2012; Wang et al., 2003; Li et al., 2017). One of the prospective red light emitters is aluminum nitride doped with Mn ions (AlN:Mn).

Aluminum nitride is a direct wide bandgap material ($E_g > 6.0$ eV) (Li et al., 2003; Feneberg et al., 2010) with the wurtzite crystalline structure, possessing numerous excellent characteristics such as high electrical insulation and thermal conductivity together with high chemical stability (Jackson et al., 1997; Abid et al., 1986). It is also non-toxic (Aluminum nitride powder, 2023; Manganese, 2023) and has good stability in corrosive environments, such as high temperatures and high energy radiation (F-UV light and X-rays) (Ettmayer and Lengauer, 2000; Polikarpov et al., 2015). These properties make it an excellent host for luminescent dopants.

The Mn^{2+} ions in AlN emit a red light peaking around 600 nm. There are two main properties characteristic of the red luminescence of AlN:Mn^{2+}, which makes the material promising as a red light emitter and attracts the attention of researchers in this field. One of them is a high value of the red luminescence quantum yield under UV light excitation (>80 %) (Polikarpov et al., 2015; Cherepy et al., 2016), and another one is recently discovered persistent luminescence (PersL), which is characteristic of the Mn emission in AlN (Xu et al., 2017; Zhang et al., 2013). A property of the PersL broadens the field of material application, including also biomedical usage.

* Corresponding author at: Institute of Solid State Physics, University of Latvia, 8 Kengaraga Str., LV-1063 Riga, Latvia.
E-mail address: baiba.berzina@cfi.lu.lv (B. Berzina).

https://doi.org/10.1016/j.rio.2023.100365
Received 17 November 2022; Received in revised form 6 January 2023; Accepted 15 January 2023
Available online 18 January 2023

Photoluminescence (PL) and excitation (PLE) spectra of AlN:Mn^{2+} are defined by the energy level structure of the Mn^{2+} ion (Corliss and Sugar, 1977) as well as by the presence of various defect types in the crystalline lattice of AlN. The direct intra-center absorption and emission of Mn^{2+} ions cause the transitions between the ground and excited energy levels of valence electrons in the $3d^5$ states. Since the d-to-d transitions are known to be spin forbidden (Lohr, 1972), the PL of AlN:Mn^{2+} under intra-center excitation has a low intensity (Cherepy et al., 2016). However, when an energy transfer from another type of excited defect to Mn^{2+} ions occurs (Li et al., 2017; Polikarpov et al., 2015; Cherepy et al., 2016), the intensity of the PL of AlN:Mn^{2+} can be greatly increased bypassing the weak direct absorption.

Luminescence of AlN:Mn^{2+} at 600 nm forms a broad band appearing in both the PL and cathodoluminescence (CL) spectra (Cherepy et al., 2016; Xu et al., 2017; Zhang et al., 2013; Wang et al., 2014; Wang et al., 2021; Sato et al., 2007). This emission is related to the transitions between the $^4T_1 \rightarrow {}^6A_1$ electronic states of Mn^{2+} ion (Wang et al., 2014; Wang et al., 2021). The PLE spectrum of 600 nm emission is made up of several weak bands appearing within the 350–550 nm spectral range (Cherepy et al., 2016; Zhang et al., 2013; Wang et al., 2021). The origin of these bands is related to the optical transitions from the $^6A_1(^6S)$ ground electronic state to the lowest excited states of Mn^{2+} ion, such as $^4T_1(^4G)$, $^4T_2(^4G)$, $^4A_1(^4G)$, $^4E(^4G)$, $^4T_2(^4D)$, and $^4E(^4D)$ (Wang et al., 2014; Wang et al., 2021). As stated before, the luminescence of Mn^{2+} ions can be successfully excited via interactions with other types of excited defects in the host material. Such interactions depend heavily on the position of Mn^{2+} ions and other defects in the crystalline lattice.

In AlN crystalline lattice, the Mn^{2+} ions substitute for the Al^{3+} ions (Miyajima et al., 2006). A distinction in the effective ion radii of Mn^{2+} and Al^{3+} (67 pm and 53 pm, respectively (Shannon, 1976) as well as a difference in its electrical charge must cause a local distortion of the crystalline lattice around the Mn^{2+} ion. This problem can be partially solved by substituting of the N^{3-} ion from a surrounding of the Mn^{2+} with a smaller O^{2-} ion (146 pm and 140 pm, respectively (Shannon, 1976).

In the crystalline lattice of AlN, there are also a variety of additional types of defects, such as Al and N vacancies (V_{Al}, V_N, respectively) and others, that can scale down the spatial and electrical charge problems noted above by being adjacent to the Mn^{2+} ions. For this purpose, one of the most appropriate complex defect is the so-called oxygen-related defect (V_{Al}–O_N). It consists of V_{Al} and oxygen ions substituting for nitrogen (O_N) – very common and always present defects in AlN (Youngman and Harris, 1990; Schweizer et al., 2000; Slack, 1973). There are several types of luminescent V_{Al}–O_N defects in the crystalline lattice of AlN (Zhou et al., 2020), forming their PLE bands in the UV part of the spectrum and PL bands in the UV – blue spectral region (Youngman and Harris, 1990; Berzina et al., 2009; Koppe et al., 2016). In addition to their own luminescence, optical excitation of the V_{Al}-O_N centers causes the energy accumulation in the crystalline lattice by filling trap levels with charged particles (Trinkler and Berzina, 2011), as well as effective excitation of Mn^{2+} ions if present in AlN, resulting in the long-lasting 600 nm emission (Xu et al., 2017; Zhang et al., 2013).

The concentration quenching of Mn luminescence in AlN:Mn^{2+} is observed. It is mostly attributed to the formation of non-radiative Mn-Mn ion pairs (Cherepy et al., 2016; Zhang et al., 2013; Wang et al., 2014; Lei et al., 2018; Shi et al., 2015). The optimal molar concentrations of Mn dopant for the highest luminescence intensity range from sub-1 % (Cherepy et al., 2016; Lei et al., 2018) to 3 % (Zhang et al., 2013; Wang et al., 2014; Shi et al., 2015).

To summarize a brief report above, there are numerous investigations of the red luminescence caused by the Mn^{2+} ions in AlN. At the same time, a comprehensive luminescence mechanism being able to explain a variety of the main experimental results related to AlN:Mn emission still needs to be developed. Our group has been working on spectral characterization of AlN material for many years. The present investigation is devoted to the spectral characterization of AlN:Mn ceramics and nanopowders, including luminescence kinetics measurements. It allows to deepen the knowledge about the luminescence processes and to find out more about the detailed luminescence mechanisms. In the future, it could allow developing of the material with advisable properties available for practical application.

2. Materials and experimental

2.1. Materials

Optical properties of AlN:Mn ceramics (Cer) and nanopowders (NP) were studied. A mass concentration of Mn ions of around 1 % was chosen, fitting the optimal concentrations' interval causing the most intense Mn luminescence (Cherepy et al., 2016; Wang et al., 2014; Lei et al., 2018; Shi et al., 2015). The studied samples were prepared at Riga Technical University, Institute of Inorganic Chemistry.

For the synthesis of AlN:Mn Cer AlN powder (20 – 80 μm; purity > 99 %; STREM Chemical Inc) as raw material and metallic Mn (macro powder; purity 99.9 %; Fluka) were homogeneously mixed for 30 min. using Fritsh grinding apparatus. The prepared mixture was filled into cylindrical graphite die with a diameter of 20 mm and placed between the graphite punches in the spark plasma sintering apparatus (SPS-825 CE, Syntex Inc). During the sintering, the temperature was Increased from 20 to 800C at a rate of 100C/min and held for 10 min. After that, the temperature was Increased from 800 to 1600C at a rate of 100C/min and held for 20 min. at a pressure of 24 MPa in a vacuum. The prepared sample's surface was cleaned by polishing with the polishing machine (LaboPol-6, Struers). As a result, the Mn-doped AlN ceramics sample with a 1 % Mn mass concentration was prepared.

AlN:Mn NP with an average grain size of 60 nm was synthesized by the plasma-chemical method. High-purity aluminium macro powder (20 – 40 μm) was injected into the reactor and evaporated in high-frequency plasma (average temperature 5400 K), high purity N_2 atmosphere. A small amount of ammonia was added to the reactor to catalyse the formation of AlN and decrease the final product grain size. Doping with Mn was done by mixing nanopowder with MnO_2 and isopropanol in a pestle. The resulting product was heated up to several hundred degrees to promote Mn diffusion into the AlN matrix.

2.2. Experiment

The following procedures and set-ups were used to comprehensively characterize the AlN:Mn materials listed above.

The material structure was studied using X-ray diffraction (XRD) on a standard RIGAKU X-ray diffractometer with a Cu-Kα X-ray source.

Spectral characterization of materials was realized by measuring the photoluminescence spectra, photoluminescence excitation spectra and luminescence kinetics (LK). The PL and PLE spectra were recorded using the hand-built and industrial (spectrometer FLS1000, Edinburgh Instruments) spectral set-ups. The PL spectra were measured within a spectral interval of 250 nm – 700 nm. For the material excitation, the spectral range of 200–550 nm was covered by using either the deuterium lamp ((DL-400 W) or xenon lamp (Xe-150 W). The 263 nm emitting solid-state laser and a tunable pulsed solid-state laser Ekspla NT342/3UV (operating range 210 – 350 nm and 420–710 nm) also were used as a light source. Use of a closed cycle refrigerator (CCS-100/204, Janis Research Corporation, Advanced Research Systems ARS-4HW and DE-202SE) allowed spectral measurements at various fixed temperatures between the room temperature (RT) and 10 K. All necessary spectral corrections related to different parts of the set-up were considered.

The following procedures and set-ups were used for the luminescence kinetics studies. 1) Luminescence was excited with light from the tunable pulsed solid state-laser Ekspla NT342/3UV. The emission signal was detected by a photomultiplier tube (time resolution better than 20 ns) coupled with an Andor SR-303i-B spectrometer. 2) For detection of the long-lasting luminescence of AlN:Mn a standard equipment Lexsyg

Research TL/OSL reader (Freiberg Instruments, Germany) combined with a solid-state laser 263 nm was employed.

3. Results and discussion

3.1. Materials structure

The XRD patterns of AlN:Mn Cer and NP together with the standard XRD pattern for wurtzite AlN (01–086-4277), are shown in the Fig. 1. The line structure for all studied materials is generally coincided with the standard pattern. It confirms that wurtzite crystalline structure is characteristic and predominated in all AlN samples used in the present investigation.

Nevertheless, in the case of nanomaterials, the signs of deterioration were detected, seen as additional peaks and noisy signals in Fig. 1. It could be caused by oxidation of the nanomaterial surface or its reaction with water vapor in the air.

3.2. Spectral characterization of materials

3.2.1. Luminescence and excitation spectra at RT

Luminescence and excitation spectra of AlN:Mn Cer and NP were investigated at room temperature (RT) and depicted in Fig. 2.

The PL spectrum of AlN:Mn Cer obtained at 263 nm excitation forms intensive 600 nm emission of Mn^{2+} ions (Fig. 2, curve 5), which is dominant and appears together with other weak emission bands at 390 and 480 nm (curves 2 and 3, correspondingly), caused by the emission of the oxygen-related defects (Berzina et al., 2009) and F-centers (Berzina et al., 2020).

The PLE spectrum of 600 nm Mn luminescence of AlN:Mn Cer is complex. It consists of two parts (Fig. 2, curves 1 and 4), covering various spectral regions. One of them (curve 4) is placed within the region of visible light (430 – 540 nm) and consists of a set of sub-bands, which characterize a direct absorption of the Mn^{2+} ion caused by optical transitions between the ground state and various lowest excited states of Mn^{2+} ion (Corliss and Sugar, 1977). A structure of this spectrum is close to that observed previously (Polikarpov et al., 2015; Zhang et al., 2013; Wang et al., 2014; Wang et al., 2021; Lei et al., 2018; Shi et al., 2015). Another part of the PLE spectrum of Mn ions excitation (Fig. 2, curve 1) is located within the UV spectral region and consists of two sub-bands peaking at 245 and 280 nm. This spectral interval covers absorptions related to uncontrollable native defects, characteristic and always-present in the crystalline lattice of AlN, including the oxygen-related defects (Youngman and Harris, 1990; Schweizer et al., 2000; Slack, 1973; Zhou et al., 2020; Berzina et al., 2009; Koppe et al., 2016; Trinkler and Berzina, 2011; Trinkler et al., 2021) as the most important among others. As seen from this figure, the efficiency of Mn^{2+} ions excitation through energy transfer from these excited defects is high, in comparison with what appeared under direct excitation of Mn^{2+} ions, thus it presents a good agreement with the results reported previously (Polikarpov et al., 2015; Cherepy et al., 2016; Xu et al., 2017).

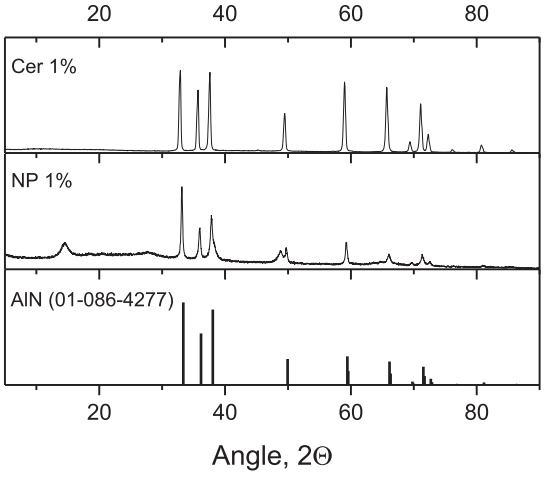

Fig. 1. The XRD patterns for AlN:Mn Cer and NP together with a standard XRD pattern for wurtzite AlN (01–086-4277).

The PL spectra of AlN:Mn Cer were measured under excitation with light from both the 245 nm and 280 nm sub-bands. It is observed that for each of these excitations, the shape of normalized 600 nm PL band coincides with those observed at 263 nm excitation, while the emission spectra of native defects are different (Fig. 2, curves 2, and 3).

The PL spectrum of AlN:Mn NP was measured under 263 nm excitation, and the shape of the 600 nm band perfectly matches the curve observed for AlN:Mn Cer (Fig. 2, the black points on curve 5). Nevertheless, in the case of NP, the intensity of 600 nm PL is many times lower than that observed for the Cer.

The obtained results demonstrates the presence of two ways for the origination of the luminescence of Mn^{2+} ions in AlN. One of them is the so-called intra-center luminescence (ICL). It takes place when absorption of exciting light and following emission occur directly inside the Mn^{2+} ion. As discussed above, the PLE spectrum of intra-center luminescence of Mn ions is located within the visible spectral region (Fig. 2, curve 4). In the present investigation, a light from the sub-band at around 520 nm (related to the $^6A_1 \rightarrow {}^4T_2$ (^4G) transition in Mn^{2+}) was used for excitation of the ICL. Another way for origination of the Mn^{2+} luminescence is more complicated when several other defects' types are involved in this process, causing the so-called recombination luminescence (RecL). For the realization of the RecL, at least two different defects are necessary – one of them absorbs exciting light, but other one (Mn ion) –realizes emission, including the energy transfer process between the involved defects. In the case of AlN:Mn, the 600 nm RecL of Mn^{2+} ions occurs under the sample irradiation with UV light, resulting in the direct excitation of native defects (Fig. 2, curve 1).

3.2.2. Temperature-dependent Mn luminescence

600 nm Mn luminescence spectra of AlN:Mn Cer excited either at 520 nm or 263 nm are studied at different fixed temperatures within an interval of 10–300 K (RT), as shown in Fig. 3, a and b. The first excitation causes the ICL processes, whereas the second one – a more complicated RecL. A fine structure of the PL spectra appears at low temperatures within a region 10 – 200 K for excitation at both: 520 nm and 263 nm. Such fine structure of the PL spectra was observed previously at 18 K (Sato et al., 2007). In the present investigation the fine structure of the PL spectra largely disappears at temperatures above 200 K; nevertheless, its small traces can be noticed even at RT (Fig. 3, a and b; Fig. 2, curve 5). The most likely, these small peaks could be related to the phonon-induced replicas (Carlone et al., 1984).

The dependence of 600 nm Mn luminescence intensity on temperature is studied. At each fixed temperature, the integral intensity of Mn ion emission (I_{lum}) is estimated as an area under the PL curve extending within the spectral interval 570–620 nm, as represented in Fig. 3, a, and b. The dependence of I_{lum} on the temperature at 520 and 263 nm excitations is depicted in Fig. 3, c. As can be seen, an excitation of the Mn ions at 520 nm results in the increase in luminescence intensity with the decrease in temperature from 300 to 10 K. The Arrhenius plot of this dependence (Fig. 3, d) demonstrates a typical picture, which is characteristic of intra-center luminescence caused by the temperature-sensitive non-radiative transitions between the energy levels of the luminescence center (Stepanov and Gribkovskii, 1968). Two temperature regions are selected between either the RT and 200 K, or 40 K – 10 K, where the representing graphic conforms to a straight line. It allows conclusion, that at high temperatures, the growth of I_{lum} with a decrease in temperature could be described with an exponential function, thus demonstrating a temperature dependent "freezing" of non-radiative transitions between the excited and ground energy states of Mn^{2+} ion. These non-radiative transitions completely freeze, when the low-

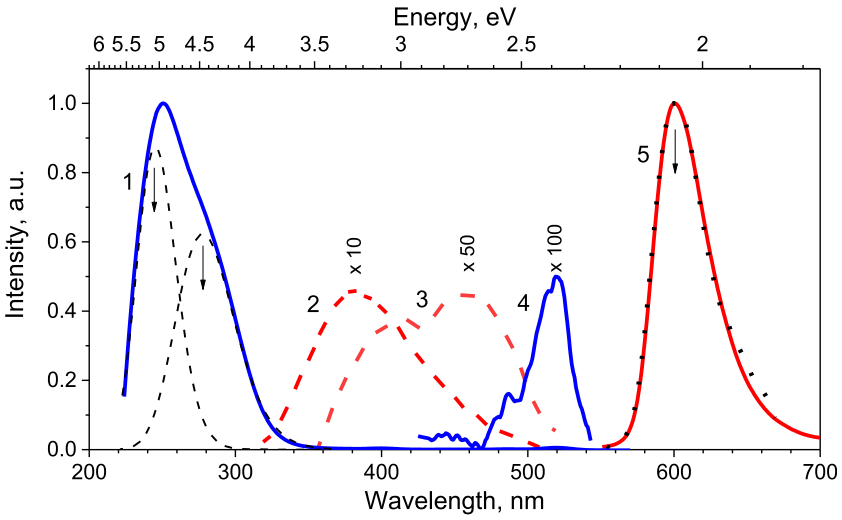

Fig. 2. Normalized PL and PLE spectra of AlN:Mn^{2+} Cer; RT. Red curves – the PL spectra, and blue curves – the PLE spectra. 1 and 4 – the PLE spectra of 600 nm Mn luminescence; curve 1 is decomposed into two sub-bands peaking at 245 nm and 280 nm. 2 and 3 – oxygen defect caused luminescence under excitation at 245 nm and 280 nm, correspondingly. 5 – Mn ion caused luminescence at 263 nm excitation. The shape of 600 nm PL under 245 nm and 280 nm excitation coincides perfectly with that of curve 5. The black points on curve 5 represent the PL spectrum of AlN:Mn NP under 263 nm excitation, measured under the same experimental conditions. Curves 2, 3 and 4 are scaled up for 10, 50 and 100 times, correspondingly, concerning the measurement.

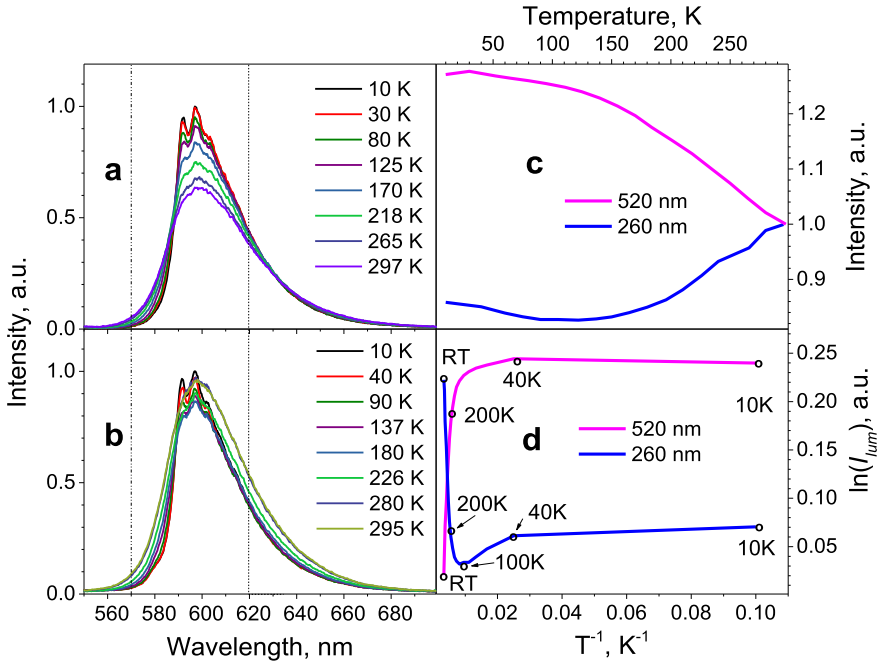

Fig. 3. PL spectra of AlN:Mn Cer measured at different fixed temperatures between 10 and 300 K under the following excitations: a – 520 nm and b – 263 nm; c – dependence on temperature of luminescence intensity (I_{lum}) measured at 520 and 263 nm excitation. d – Arrhenius plot of the results depicted on the section c. The dash lines on the sections a) and b) limit a spectral interval for which the I_{lum} is evaluated.

temperature region below 40 K was reached, maintaining a constant value of luminescence intensity at lower temperatures.

On the contrary, when the 600 nm luminescence is excited at 263 nm, and the RecL processes take place, the picture was quite different. In this case, the decrease of temperature from the RT down to 100 K results in diminishing of luminescence intensity, whereas a further decrease of temperature causes a small growth of luminescence intensity (Fig. 3, c). The Arrhenius plot of this dependence demonstrates a complicated picture (Fig. 3, d). Inside the temperature interval between the RT and 200 K, a decrease of luminescence intensity approximates with a straight line, thus characterizing the process, which is described with an exponential function. Subsequent diminishing of temperature from 200 K down to 100 K results in an increase of luminescence intensity with its further small increase down to 10 K. That complicated picture presents evidence that the RecL originates by the actions of different luminescence mechanisms, which will be discussed below.

3.2.3. *Time-dependent rise of luminescence intensity*

Growth of intensity of the 600 nm Mn luminescence during the steady-state irradiation of AlN:Mn Cer with 263 nm light, causing the RecL, is observed (Fig. 4, red curve), demonstrating the presence of complicated processes, which could be distributed into three stages. In the beginning, a fast increase of the 600 nm luminescence takes place in less than one second. Then a slower process of luminescence increase follows, lasting up to ~ 600 s. In continuation, a slow increase of luminescence intensity is in progress lasting up to the end of the measurement at ~ 3000 s.

In the case of the 390 nm luminescence caused by the oxygen-related defects, a picture of rise of the luminescence intensity is quite different (Fig. 4, the blue curve) - then, a slow decrease in luminescence intensity follows just after its fast increase at the very beginning of the measurement. It allows conclusion that both the 600 nm emission of Mn ions and 390 nm emission of oxygen-related defects are caused by different

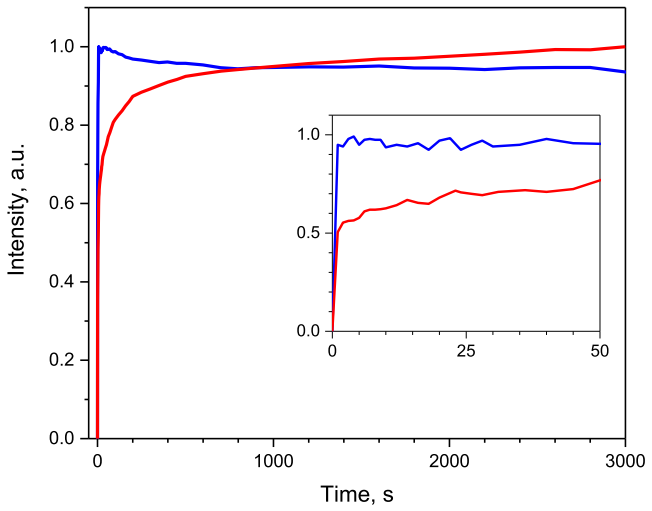

Fig. 4. AlN:Mn Cer; RT. Dependence of the intensities of 600 nm luminescence (red curve) and 390 nm luminescence (blue curve) from the duration of steady-state irradiation with 263 nm light. The inset – more detailed sight on this picture at the beginning of the sample irradiation.

processes, without direct influence from one to the other.

3.3. Luminescence kinetics

3.3.1. The fast luminescence decay

The fast decay of the 600 nm PL of AlN:Mn Cer lasting in a millisecond time scale was studied at RT. The sample was irradiated with light pulses of 5 ns duration, emitted from the tunable solid-state laser. The results of 600 nm Mn luminescence decay, obtained using the selected excitation wavelengths at 520 and 260 nm, are shown in Fig. 5, a, and b, demonstrating the exponential luminescence decay. The red lines on these figures display the results of mathematical treatment using the standard exponential approximation (OriginPro 2015; 1 exponential decay; Levenberg Marquardt iteration algorithm). It allows evaluation of the luminescence decay time constant τ as 1,21 ms and 1,22 ms for the 520 and 260 nm excitation, respectively. These results are close to the value of τ = 1,6 ms observed by other investigators (Polikarpov et al., 2015).

The coincidence of the decay constants of 600 nm Mn luminescence, caused either by intra-center or recombination processes, allows to conclude that in the case of RecL, an energy transfer from the primary excited defect to the Mn^{2+} ion happens very fast and did not hamper decay of the Mn^{2+} ion emission. This conclusion is undoubtedly in force at RT where the measurements were performed.

A time-dependent rise of luminescence pulses related to the used time scale is not detectable (Fig. 5, a, and b).

3.3.2. Persistent luminescence

In the present research the properties of PersL of AlN:Mn^{2+} Cer are studied at RT. The samples were irradiated with 263 nm light during 120 s. After cessation of irradiating light, 30 s was waited before the recording of the PersL signals to avoid the fluorescence signals.

The PersL characteristics for AlN:Mn^{2+} Cer are seen in Fig. 6. The 3D image of the PersL in wavelengths-time coordinates are depicted in sections b. As seen from this image, the 600 nm PersL of Mn^{2+} ions are seen during the applied period of 1000 s. Besides the Mn luminescence, another long-lasting emission of the oxygen-related defects at 390/480 nm also is observed. From this 3D image (Fig. 6, b), two PersL emission spectra are constructed at two fixed points on the time scale, when 35 s and 500 s were passed from the starting point of the measurement, and the normalized spectra are depicted on Fig. 6, a. These spectra consist of the bands at 600 nm, 480 nm and 390 nm, and the shape of the Mn^{2+} caused 600 nm emission does not change during this time. A decay of the

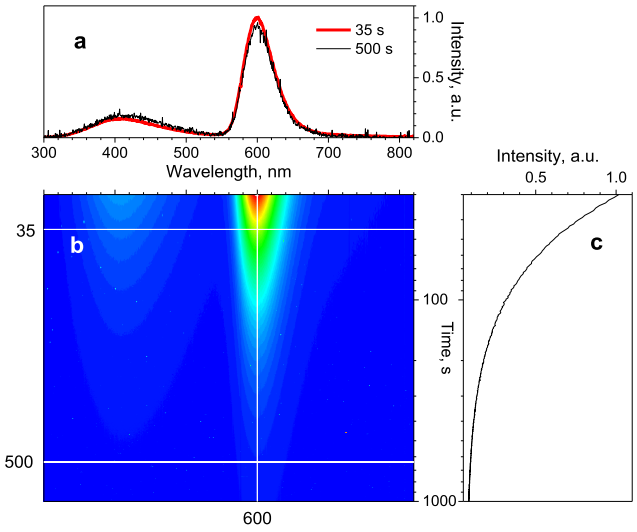

Fig. 6. AlN:Mn Cer; RT. PersL caused by 120 s irradiation with 263 nm light; a – normalized PersL spectra measured at 35 s and 500 s after the beginning of PersL recording; b – 3D image of PersL in wavelengths-time coordinates; c – long-lasting decay of 600 nm PersL.

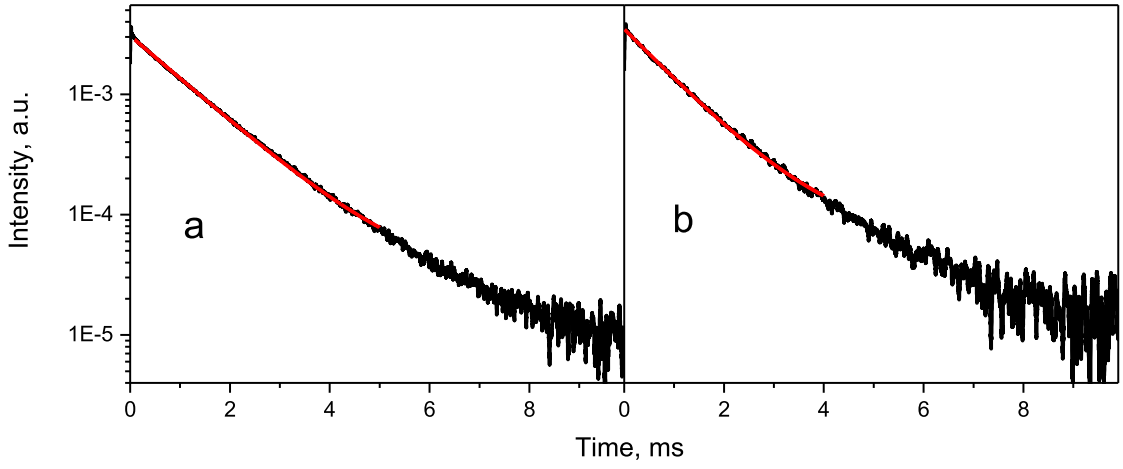

Fig. 5. AlN:Mn Cer; RT. The 600 nm luminescence decay measured under excitation with 5 ns laser pulse at: a) 520 nm, and b) 260 nm.

intensity of 600 nm emission is shown in Fig. 6, c.

More detailed measurement of the decay of 600 nm PersL of AlN:Mn Cer lasting up to 7000 s is shown in Fig. 7. It was found that the conventional three-exponential functions approximation fitted well the experimental luminescence decay, forming a fast, intermediate and slow components characterized with the decay constants $\tau_1 = 44$ s, $\tau_2 = 285$ s and $\tau_3 = 1650$ s, respectively.

PersL properties for AlN:Mn^{2+} nanopowders also were studied. In this case, a results packet, analogous to that depicted in Fig. 6 for AlN:Mn^{2+} Cer, was obtained, therefore it is not demonstrated as an individual figure. A difference observed for these materials is in intensity of the PersL. The PersL intensity emitted by nanopowder is lower than that observed in ceramics. This probably occurred due to different doping temperatures – in case of Cer doping was done at 1600C, but in case of NP – only at several hundred degrees C (2.1. Materials). As a result Mn diffusion into AlN NP matrix was likely of smaller extent – Mn concentration in NP was lower than in Cer.

3.4. Luminescence mechanisms

The results discussed above allow the construction of the main luminescence processes together with the proposal of appropriate luminescence mechanisms.

For a better understanding of the processes resulting in Mn^{2+} luminescence and interpretation of the experimental results, the energy level scheme of AlN:Mn^{2+} is constructed and depicted in Fig. 8. It contains the valence band (VB) and conduction band (CB) of the AlN host together with the energy level structure of some defects, which were essential for the ongoing processes. The main of them are the oxygen-related defects (V_{Al}-O_N), separate oxygen ions and Mn^{2+} ions. These defects forms their energy levels, consisting of the ground energy state and excited states located inside the bandgap. In Fig. 8, the ground state energy levels of the examined defects are marked with odd numbers, while the excited states – with even numbers, correspondingly. Besides, in that scheme, the number 8 labels the energy levels of various traps for electrons, whereas the number 7 – the same for the holes. As it is known, there are several variations of the V_{Al}-O_N centers characteristic for the AlN (Zhou et al., 2020), and most of them absorb UV-light around 260 nm with the following emission around 390 nm or 480 nm (Berzina et al., 2009).

The structure of such an energy level scheme is based on the results of previous investigations of luminescence of oxygen-related defect in AlN (Youngman and Harris, 1990; Schweizer et al., 2000; Slack, 1973; Berzina et al., 2009; Berzina et al., 2002; Berzina et al., 2000; Trinkler et al., 2002; Berzina et al., 2009; Trinkler and Berzina, 2014; Trinkler and Berzina, 2014; Trinkler et al., 2021). It allowed the location of the excited state of the V_{Al}-O_N center as contacting or partly overlapping with the bottom of the conduction band. This assumption is based on the experimental fact that excitation of this center by the UV light around 260 nm results in the emission of characteristic 390/480 nm light, and also provides energy storage in material, thus manifesting the presence of free electrons within the CB. These electrons have been released from the excited V_{Al}-O_N centers and afterwards captured on the appropriate trap centers (transitions 2 → 8, Fig. 8), and this process was observed even at low temperatures (Trinkler and Berzina, 2014).

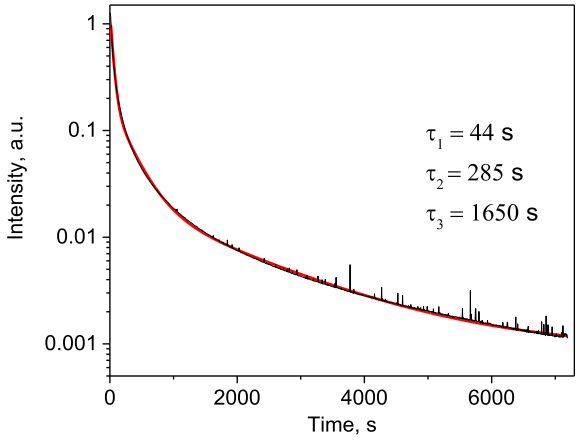

Fig. 7. AlN:Mn Cer; RT; decay of 600 nm PersL caused by irradiation of 263 nm light during of 120 s. The black curve – experimental results; the red curve – fitted results using of three exponential functions with decay times: τ_1, τ_2, and τ_3.

Similar but not analogous and so complicated energy level schemes for elucidation of AlN:Mn luminescence can also be found in works (Wang et al., 2014; Wang et al., 2021).

The intra-center luminescence of Mn^{2+} ions in AlN:Mn is depicted in Fig. 8, involving the transitions 5 → 6, which characterize the absorption of 520 nm light and the following 600 nm emission (transitions 6 → 5).

Recombination luminescence of Mn^{2+} ions in AlN:Mn takes place when the defects, which are responsible for light absorption and luminescence emission, are different. As followed from the spectral measurements depicted in Fig. 2 and those of the previously reported (Cherepy et al., 2016; Xu et al., 2017; Trinkler and Berzina, 2011), the 600 nm Mn^{2+} luminescence is realized with high efficiency by means of the direct excitation of the oxygen-related defects absorbing light around 260 nm. According to the energy level scheme from Fig. 8, absorption of the 263 nm light is depicted as the transitions between the ground and excited states of the $V_{Al} - O_N$ center (1 → 2), but the 600 nm emission - as the transitions between the excited and ground energy levels (6 → 5) of Mn^{2+} ion. Therefore, the energy transfer between the excited $V_{Al} - O_N$ center and luminescent Mn^{2+} ion is necessary. Two basic mechanisms for this energy transfer exist. One of them includes ionization of the primary excited center (transition 2 → CB) with a subsequent capture of the released electron on the excited states of Mn^{2+} ion (CB → 6). For the realization of the emission of Mn^{2+} ion (6 → 5), simultaneous capture of a hole (VB → 5, 1 → 5 or 7 → 5) is necessary. This mechanism depends on temperature and hereafter is named "recombination luminescence with ionization" with the acronym RLI. Another mechanism relates to the tunnel processes (with the acronym RLT) (Delbecq et al., 1974). In Fig. 8 the RLT is labelled by transitions between the energy levels of the primary excited defect to the excited states of Mn^{2+} ion including the necessary hole processes (2 → 6; together with 1 → 5; 7 → 5; VB → 5). Usually, the tunnel processes are temperature-independent; nevertheless, thermo-assisted tunneling is also possible (Vedda and Fasoli, 2018).

The RecL processes in AlN:Mn are quite complicated as followed from the measurements of luminescence kinetics (Fig. 5, b; Figs. 6, and 7), time-dependent rise of luminescence intensity (Fig. 4) and temperature-dependent luminescence spectra (Fig. 3, c, and d). Engagement of different luminescence mechanisms (RLI or RLT) can vary during the time scale and depend on the sample's temperature. The time scale, where the 600 nm RecL of AlN:Mn under 263 nm excitation is observable, is huge, beginning from the milliseconds (Fig. 5, b) and lasting up to ~ 7000 s (Fig. 7) and longer (Cherepy et al., 2016; Xu et al., 2017), therefore, various mechanisms could prevail within the different periods of the time scale.

The fast RecL, resulting in the emission of Mn^{2+} ions, appears during irradiation of the sample with 263 nm light. As discussed above, a decay of the fast RecL at RT lasts within a time scale of milliseconds, and its decay constant (τ = 1,2 ms) coincides with that observed for the intra-center luminescence (Fig. 5, a, and b). It allows estimation of the energy transfer time from the primary excited defect to the luminescent - Mn^{2+} ion as being very fast, which does not attain the millisecond time scale. The fast processes are characteristic for the RLT mechanism. Nevertheless, as seen from Fig. 3. c, a decrease of the temperature downwards the RT results in a reduction of the 600 nm RecL intensity, which is opposite to the increase of the ICL intensity, measured under

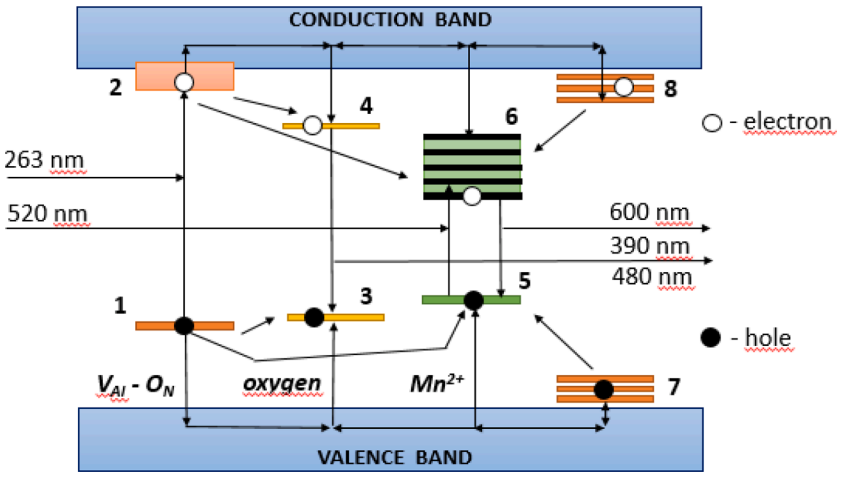

Fig. 8. An energy level scheme of AlN:Mn illustrating the luminescence processes and proposed mechanisms. A detailed description of this scheme can be found in the text.

the same experimental conditions, thus manifesting an action of the fast temperature-dependent RLI process, which was partly stopped at about 150 K. It allows assumption, that within a temperature region below 150 K the RLT mechanism prevails. These results suggest, that the fast component of the 600 nm RecL of AlN:Mn observed under 263 nm excitation at RT originates by both the RLI and RLT mechanisms. A decrease in temperature results in the gradual reduction of the RLI mechanism, while at 150 K and lower temperatures, the RLT mechanism could remain as dominant.

The defect types originally absorbing the 263 nm light are important for realizing the RecL, resulting in 600 nm emission. As previously discussed, these defects could mainly be related to the oxygen-related formations, representing the native defects characteristic of the AlN crystalline lattice. There are several types of oxygen-related defects in the crystalline lattice of the AlN host (Zhou et al., 2020; Berzina et al., 2009; Koppe et al., 2016), and as follows from the PLE spectrum depicted in Fig. 2, two defect types absorbing the 263 nm light resulting in RecL of Mn^{2+} ions exist. Electrical recharging between the different defect types and their accumulation, which follow light absorption, is possible. It could be a reason for the time-dependent rise of the 600 nm luminescence intensity under 263 nm excitation demonstrated in Fig. 4.

The slow RecL or the **long-lasting PersL** of AlN:Mn^{2+} Cer covers a time scale measurable in hours at RT, and its properties are demonstrated in Figs. 6, and 7. In this case, the presence of the fast RecL discussed above is completely excluded because registration of the PersL began when the fast processes were over. A decay curve of the 600 nm PersL, depicted in Fig. 7, is complicated, and it could be described with three different exponents characterized by distinctive decay constants. It allows the assumption that at least three main but differing time-dependent processes originating the PersL exist. Most credibly, these processes could be based on variations of the defect types involved in the formation of the RecL. These variations of defects could be caused by the transformations that follow irradiation of the material with the 263 nm light, and their lifetimes could be different. As known, irradiation of the material with 263 nm light did not create new defects but solely results in the electrical recharging of existing defects. Filling of the traps for electrons or holes with appropriately charged particles (Fig. 8, transitions CB → 8 and VB → 7, correspondingly) is one of these processes. The less stable of these defects disappear during a relatively short time, forming the first two components of the PersL decay (Fig. 7). As discussed above, the mechanisms resulting in RecL emission are highly dependent on temperature, and at RT they see include both the RLT and RLI mechanisms.

The most tentatively, the long-lasting component of the PersL, which is described with the third decay component (Fig. 7), can be related to the thermo-stimulated processes realizing through the RLI mechanism (Fig. 8, transitions 8 → CB → 6, and VB → 5 for electrons and holes, correspondingly), however, concurrent participation of thermo-stimulated tunneling completely cannot be excluded (Fig. 8, transitions 8 → 6 and 7 → 5). The origin of the long–lasting component of the PersL seems to be the same as for the thermo-stimulated luminescence (TL). The TL measurements are not included in the present study.

According to the RLI mechanism, which is fundamental for both the long-lasting PersL and TL, an action of the electron-hole pair is necessary for causing the emission of the Mn^{2+} ion. This mechanism realizes (Fig. 8) when an electron from the CB, which is previously thermally released from the trap state (8 → CB), is attached to the excited states of the Mn ion (CB → 6). As a result of the described process, a change of the electrical charge of Mn ion from + 2 to + 1 had to follow, but it does not happen, and the 600 nm emission of Mn^{2+} ions appears (Figs. 2 and 7). This discrepancy could be treated by capturing a hole in the Mn^{2+} ion (Fig. 8, transitions 7 → VB → 5). It could be expected that this process should realize either just before or simultaneously while capturing an electron to the excited states of the Mn ion. As a result, the valence of excited Mn ion remains unchanged, and 600 nm emission of Mn^{2+} ions appears. Similar cooperation of the electrons and holes seems necessary when the RLT mechanism caused RecL of Mn ions and transitions between the energy levels 8 → 6 or 7 → 5, depicted in Fig. 8, also are involved.

In the AlN material, at least two groups of the hole centers could be distributed, and those could participate in forming of the long-lasting PersL. The first of them could be related to individual traps for holes, which were caused by randomly distributed native defects of the host material, forming their energy levels above the top of the valence band (Fig. 8, levels 7). The second group includes the defects of the crystalline lattice, which form close pairs with the Mn^{2+} ions and could stimulate an ionization of the Mn ion. The bivalent O_N ions and their varieties could be selected as the most important candidates for forming close pairs with Mn^{2+} ions. On the one hand, such defect association in pairs in the crystalline lattice of AlN compensates for the local electrical charge. On the other hand, a difference in the ion radii, relating to the basic elements of the host material and those of the Mn and O_N impurities (discussed in section 1), also could stimulate a close location of these two ions in the crystalline lattice. In general, such an approach elucidates the high efficiency of 600 nm luminescence, which appears at 260 nm excitation (Fig. 2, and (Polikarpov et al., 2015; Cherepy et al., 2016; Xu et al., 2017).

As reported above, there are no differences in PL spectra and PersL characteristics when measured for AlN:Mn^{2+} Cer and nanopowders.

Recently, similar PersL properties of Eu^{2+} luminescence in AlN:Eu^{2+}

ceramics were observed (Berzina et al., 2022). These results together with those discussed above for AlN:Mn^{2+} allow the conclusion that exactly the host material structure, which always contains native defects such as the oxygen-related ones and others, mainly is responsible for the PersL properties, whereas the various luminescent dopants such as Mn^{2+} or Eu^{2+} ions serve as emitters and indicators of the long-lasting processes.

4. Summary

The 600 nm luminescence caused by the Mn^{2+} ions is studied in AlN:Mn ceramics using spectral methods of investigation, including measurements of luminescence kinetics and studies of PersL properties. The PersL properties for AlN:Mn nanopowders are studied too. The main activities and results are the following.

1. Luminescence of Mn^{2+} ions in AlN:Mn Cer was studied when the 600 nm emission was recorded during an irradiation of the sample either with 263 nm light resulting in excitation of the oxygen-related defects or with 520 nm light directly exciting the Mn^{2+} ions. In the first case, the 600 nm emission could be characterized as recombination luminescence, whereas, the 520 nm excitation causes the intracenter luminescence of Mn^{2+} ions. It was observed that at RT, these photoluminescence spectra of the RecL and ICL coincide (Fig. 2).
2. In AlN:Mn Cer, the luminescence decay of the RecL and ICL at RT was studied. In both cases, the 600 nm luminescence decay lasts within a timescale of milliseconds, and the characteristic luminescence decay constants ($\tau = 1{,}2$ ms) coincide (Fig. 5, a, and b). It allows concluding that in the case of RecL the energy transfer process from the primary excited oxygen-related defect to the emitting Mn^{2+} ion was fast.
3. In AlN:Mn Cer the properties of the fast RecL were studied, including measurements of 600 nm luminescence intensity at different fixed temperatures within an interval from RT down to 10 K (Fig. 3, c) and time-dependent rise of luminescence intensity at RT (Fig. 4). It allows evaluation of the action of the mechanisms responsible for the origination of the fast RecL. Two main mechanisms are based either on the ionization of the primary excited defects (RLI) or the tunneling processes between the defects (RLT) causing the 600 nm emission of Mn^{2+} ions. It allows propose that both mechanisms coexisted at RT, and the role of the RLI mechanism diminished with a decrease in the sample temperature. In contrast, at ~ 150 K and lower temperatures, the RLT mechanism become prevalent. It is suggested that to realize both the RLI and RLT mechanisms, the participation of the electron-hole pairs is necessary.
4. In AlN:Mn Cer, the properties of the long-lasting PersL were studied at RT. It is observed that the shape and spectral location of the 600 nm Mn^{2+} emission band remains unchanged at different points from luminescence afterglow (Fig. 6, a). The decay of the PersL was measured down to 7000 s (Fig. 7). This PersL decay could be described with three exponential functions with different decay constants τ evaluated as 44 s, 285 s, and 1650 s. It demonstrates the complex character of the PersL processes, including the contribution of recombination luminescence mechanisms and the role of time-dependent transformations of excited defects. It could be suggested that the origin of the longest component of the PersL is the same as for the thermo-stimulated luminescence, which is realized via the thermal release of trapped electrons and holes accumulated in the material during its initial irradiation with 263 nm light.

Similar characteristics of the 600 nm PersL, obtained for the AlN:Mn^{2+} Cer, were observed for the nanopowders.

CRediT authorship contribution statement

R. Ruska: Investigation, Writing – original draft, Conceptualization. **B. Berzina:** Conceptualization, Investigation, Writing – original draft, Supervision, Project administration, Funding acquisition. **J. Cipa:** Methodology, Investigation. **L. Trinkler:** Methodology, Investigation, Writing – review & editing. **A. Sarakovskis:** Conceptualization, Investigation. **J. Grabis:** . **I. Steins:** .

Declaration of Competing Interest

The authors declare that they have no known competing financial interests or personal relationships that could have appeared to influence the work reported in this paper.

Data availability

Data will be made available on request.

Acknowledgments

This research is funded by the Latvian Council of Science grant No. LZP (FLPP)-2019/1–0443. Institute of Solid State Physics, University of Latvia as the Center of Excellence has received funding from the European Union's Horizon 2020 Framework Programme H2020-WIDESPREAD-01-2016-2017-Teaming Phase 2 under grant agreement No. 739508, project CAMART2.

References

Abid, A., Bensalem, R., Sealy, B.J., 1986. The thermal stability of AlN. J. Mat. Sci. 21 (4), 1301–1304.
Aluminum nitride powder, 10 μm, ≥98% | Sigma-Aldrich, https://www.sigmaaldrich.com/catalog/product/aldrich/241903?lang=en&region=LV.
Berzina, B., Trinkler, L., Sils, J., Palcevskis, E., 2000. Oxygen-related defects and energy accumulation in AlN ceramics. Rad. Effects Defects in Solids 156, 241. https://doi.org/10.1080/10420150108216900.
Berzina, B., Trinkler, L., Sils, J., Atobe, K., 2002. Luminescence mechanisms of oxygen-related defects in AlN. Rad. Effects Defects in Solids 157 (6-12), 1089–1092.
Berzina, B., Trinkler, L., Jakimovica, D., Korsaks, V., Grabis, J., Steins, I., Palcevskis, E., Bellucci, S., Le-Chyong Chen, S., Chattopadhyay, K.-H., 2009. Spectral characterization of bulk and nanostructured aluminum nitride. J. Nanophotonics 3, 031950. https://doi.org/10.1117/1.3276803.
Berzina, B., Trinkler, L., Jakimovica, D., Korsaks, V., Grabis, J., Steins, I., Palcevskis, E., Bellucci, S., Chen, L.-C., Chattopadhyay, S., Chen, K., 2009. Spectral characterization of bulk and nanostructured aluminum nitride. J. Nanophotonics 3. https://doi.org/10.1117/1.3276803.
Berzina, B., Trinkler, L., Korsaks, V., Ruska, R., 2020. Nitrogen vacancy type defect luminescence of AlN nanopowder. Opt. Mater. 108, 110069 https://doi.org/10.1016/j.optmat.2020.110069.
Berzina, B., Ruska, R., Cipa, J., Trinkler, L., Sarakovskis, A., Grabis, J., Steins, I., 2022. Luminescence of AlN: Eu ceramics: Properties and machanisms. Opt. Mater. 127, 112217 https://doi.org/10.1016/j.optmat.2022.112217.
Carlone, C., Lakin, K.M., Shanks, H.R., 1984. Optical phonons of aluminium nitride. J. Appl. Phys. 55, 4010. https://doi.org/10.1063/1.332989.
Cherepy, N.J., Payne, S.A., Harvey, N.M., Aberg, D., Seeley, Z.M., Holliday, K.S., Tran, I. C., Zhou, F., Martinez, H.P., Demeyer, J.M., Drobshoff, A.D., Srivastava, A.M., Camardello, S.J., Camanzo, H.A., Schlagel, D.L., Lograsso, T.A., 2016. Red-emitting manganese-doped aluminium nitride phosphor. J. Opt. Mat. 54, 14. https://doi.org/10.1016/j.optmat.2016.02.008.
Corliss, C., Sugar, J., 1977. Energy levels of manganese, Mn I through Mn XXV. J. Phys. Chem. Reference Data 6 (4), 1253–1329.
Delbecq, C.J., Toyozawa, Y., Yuster, P.H., 1974. Tunneling recombination of trapped electrons and holes in KCl:AgCl and KCl:TlCl. Phys. Rev. B 9 (10), 4497–4505.
Ettmayer, P., Lengauer, W., 2000. Nitrides. In Ullmann's Encyclopedia of Industrial Chemistry; Wiley-VCH Verlag GmbH & Co. KGaA.
Feneberg, M., Leute, R.A.R., Neuschl, B., Thonke, K., Bickermann, M., 2010. High-excitation and high-resolution photoluminescence spectra of bulk AlN. Phys. Rev. B 82 (7), 075208. https://doi.org/10.1103/PhysRevB.82.075208.
Hou, D., Liu, C., Kuang, X., Liang, H., 2012, Enhanced emission of Mn^{2+} via $Ce^{3+} \rightarrow Mn^{2+}$ energy transfer in α-$Sr_2P_2O_7$, Opt. Soc. of America 20 (No27)/ Optics Express 28969.
Jackson, T.B., Virkar, A.V., More, K.L., Dinwiddie, R.B., Cutler, R.A., 1997. High-thermal-conductivity aluminum nitride ceramics: the effect of thermodynamic, kinetic, and microstructural factors. J. Am. Ceram. Soc. 80, 1421. https://doi.org/10.1111/j.1151-2916.1997.tb03000.x.
Koppe, T., Hofsass, H., Vetter, U., 2016. Overview of band edge and defect related luminescence in aluminium nitride. J. Lumin. 178, 267. https://doi.org/10.1016/j.jlumin.2016.05.055.
Lei, F., Lei, X., Ye, Z., Zhao, N., Yang, X., Shi, Z., Yang, H., 2018. Photoluminescent properties of AlN: Mn^{2+} phosphors. J. Alloy. Compd. 763, 466. https://doi.org/10.1016/J.JALLCOM.2018.05.291.

Lei, B., Liu, Y., Ye, Z., Shi, C., 2004. Luminescence properties of $CdSiO_3$:Mn^{2+} phosphor. J. Lumin. 109, 215. https://doi.org/10.1016/j.lumin.2004.02.010.
Li, J., Nam, K.B., Nakarmi, M.L., Lin, J.Y., Jiang, H.X., Carrier, P., Wei, S.-H., 2003. Band Structure and Fundamental Optical Transitions in Wurtzite AlN. Appl. Phys. Lett. 83 (25), 5163–5165.
Li, Y., Qi, S., Li, P., Wang, Z., 2017. Research progress of Mn doped phosphors. RSC Adv. 7, 38318. https://doi.org/10.1039/c7ra006026b.
Lohr, L.L., 1972. Spin-forbidden electronic excitations in transition metal complexes. Coord. Chem. Rev. 8 (3), 241–259.
Manganese (IV) oxide ReagentPlus®, >= 99 % | 1313-13-9 | Sigma-Aldrich, https://www.sigmaaldrich.com/catalog/product/sigald/243442?lang=en&region=LV.
Miyajima, T., Kudo, Y., Uruga, T., Hara, K., 2006. Analysis of the local structure of AlN: Mn using X-Ray absorption fine structure measurements. Phys. Stat. Sol. (c) 3 (6), 1742–1745.
Ni, J., Liu, Q., Wan, J., Liu, G., Zhou, Z., Xu, F., Zeng, X., Xie, R., 2018. Novel luminescent properties and thermal stability of non-rare-earth Ca-α-sialon:Mn^{2+} phosphor. J. Lumin. 202, 514. https://doi.org/10.1016/j.lumin.2018.05.042.
Polikarpov, E., Catalini, D., Padmaperuma, A., Das, P., Lemmon, T., Arey, B., Fernandez, C.A., 2015. A high efficiency rare earth-free orange emitting phosphor. J. Opt. Mat. 46, 618. https://doi.org/10.1016/j.optmat.2015.04.013.
Sato, A., Azumada, K., Atsumori, T., Hara, K., 2007. Characterozation of AlN: Mn thin film phosphors prepared by metalorganic chemical vapor deposition. J. Crystal Growth 298, 379. https://doi.org/10.1016/j.jcrysgro.2006.10.042.
Schweizer, S., Rogulis, U., Spaeth, J.-M., Trinkler, L., Berzina, B., 2000, Investigation of oxygen-related luminescence centres in AlN ceramics, Phys. Stat. Sol. (b), 219, No. (1)171, doi: org/10.1002/1521-3951(200005)219:1<171:AID-PSSB171>3.0.CO;2-0.
Shannon, R.D., 1976. Revised effective ionic radii and systematic studies of interatomic distances in halides and chalcogenides. Acta Cryst. 32 (5), 751–767.
Shi, Z., Zou, Y., Jing, R., Zhang, K., Qiao, G., Wang, H., 2015. Red-emitting AlN:Mn^{2+} phosphors prepared by combustion synthesis. Funct. Mater. Lett. 8 (2) https://doi.org/10.1142/S1793604715500253.
Slack, G.A., 1973. Nonmetallic Crystals with High Thermal Conductivity. J. Phys. Chem. Solid 34 (2), 321–335.
Stepanov, B.I., Gribkovskii, V.P., 1968. Theory of luminescence. A Book. Gordon and Breach Publishing Group.
Tanaka, M., Qi, J., Masumoto, Y., 2000. Compsrison of energy levels of Mn^{2+} in nanosized and bulk Zns crystals. J. Lumin. 87–89, 472. https://doi.org/10.1016/s0022-2313(99)00212-4.
Trinkler, L., Berzina, B., 2011. Luminescence properties in AlN ceramics and its potential application for solid state dosimetry. In: Book: Advances in Ceramics – Characterization, Raw Materials, Processing, Properties, Degradation and Healing. Publisher, InTech, pp. 59–82. https://doi.org/10.5772/18658.
Trinkler, L., Berzina, B., 2014. Recombination luminescence od aluminium nitride ceramics. Phys. Stat. Solidi B 251, 542. https://doi.org/10.1002/PSSB.201350090.
Trinkler, L., Berzina, B., 2014. Recombination luminescence in aluminium nitride ceramics. Phys. Stat. Solidi B 251, 542. https://doi.org/10.1002/PSSB.201350090.
Trinkler, L., Berzina, B., 2014. Localized transitions in luminescence of AlN ceramics. Radiat. Meas. 71, 232. https://doi.org/10.1016/j.radmeas.2014.02.016.
Trinkler, L., Botter-Jensen, L., Berzina, B., 2002. Aluminum nitride ceramics: A potential UV dosimeter material. Radiat. Protect. Dosim. 100 (N 1–4), 313. https://doi.org/10.1093/oxfordjournals.rpd.a005876.
Trinkler, L., Trukhin, A., Cipa, J., Berzina, B., 2021. UV light induced processes in pure and doped AlN ceramics. Opt. Mater. 121, 111550 https://doi.org/10.1016/j.optmat.2021.111550.
Vedda, A., Fasoli, M., 2018. Tunneling recombination in scintillators, phosphors, and dosimeters. Radiat. Measur. 118, 86. https://doi.org/10.1016/j.radmeas.2018.08.003.
Wang, X., Jia, D., Yen, W.M., 2003. Mn^{2+} activated green, yellow and red long persistent phosphors. J. Lumin. 102–103, 34. https://doi.org/10.1016/S0022-2313(02)00541-0.
Wang, X.-J., Xie, R.-J., Dierre, B., Takeda, T., Suehiro, T., Hirosaki, N., Sekiguchi, T., Li, H., Sun, Z., 2014. A novel and high brightness AlN:Mn^{2+} red phosphor for field emission displays. Dalton Trans. 43, 6120. https://doi.org/10.1039/c3dt53532k.
Wang, Q., Yang, J., Li, J., Yang, H., Feng, Z., Ge, Z., Zhang, J., Lin, Y., Wang, X., Wang, C., Fu, Y., Liu, C., 2021. Synthesis, Magnetism and photoluminescence of Mn doped AlN nanowires. Res. Square. https://doi.org/10.21203/rs.3.rs-763003/v1.
Wu, S., Li, Y., Ding, W., Xu, L., Ma, Y., Zhang, L., 2020. Recent advances of persistent luminescence nanoparticles in bioapplications. Nano-Micro Lett. 12, 70. https://doi.org/10.1007/s40820-020-0404-8.
Xu, J., Cherepy, N.J., Ueda, J., Tanabe, S., 2017. Red persistent luminescence in rare earth-free AlN:Mn^{2+} phosphor. Mater. Lett. 206, 175. https://doi.org/10.1016/j.matlet.2017.07.015.
Youngman, R.A., Harris, J.H., 1990. Luminescence Studies of Oxygen-Related Defects In Aluminum Nitride. J. Am. Ceram. Soc. 73 (11), 3238–3246.
Zhang, H., Zheng, M., Lei, B., Liu, Y., Xiao, Y., Dong, H., Zhang, Y., Ye, S., 2013. Luminiscence properties of red long-lasting phosphorescence phosphor AlN:Mn^{2+}. ESC J. Solid State Sci. Technol. 2, R117–R120. https://doi.org/10.1149/2.006307jss.
Zhou, Q., Zhang, Z., Li, H., Golovynskyi, S., Tang, X.i., Wu, H., Wang, J., Li, B., 2020. Below bandgap photoluminescence of an AlN crystal: Co-existence of two different charging states of a defect center. APL Mater. 8 (8) https://doi.org/10.1063/5.0012685, 081107.
Zhuang, Y., Katayama, Y., Ueda, J., Tanabe, S., 2014. A brief review on red to near-infrared persistent luminescence in transition-metal-activated phosphors. J. Opt. Mat. 36 (11), 1907–1912.